Title

A rapid and systematic approach for the optimization of radio thin-layer chromatography resolution

Authors

Laferriere-Holloway, Travis S

Rios, Alejandra

Lu, Yingqing

et al.

Publication Date

2023

DOI

10.1016/j.chroma.2022.463656

Peer reviewed

HHS Public Access

Author manuscript

J Chromatogr A. Author manuscript; available in PMC 2024 January 04.

Published in final edited form as:

J Chromatogr A. 2023 January 04; 1687: 463656. doi:10.1016/j.chroma.2022.463656.

A rapid and systematic approach for the optimization of radio-TLC resolution

Travis S. Laferriere-Holloway[1,4], **Alejandra Rios**[2,4], **Yingqing Lu**[2,4], **Chelsea C. Okoro**[3,4], **R. Michael van Dam**[1,2,3,4]

[1]Department of Molecular & Medical Pharmacology, David Geffen School of Medicine, University of California Los Angeles (UCLA), Los Angeles, CA, USA

[2]Physics and Biology in Medicine Interdepartmental Graduate Program, UCLA, Los Angeles, CA, USA

[3]Institute for Society and Genetics, UCLA, Los Angeles, CA, USA

[4]Crump Institute for Molecular Imaging, UCLA, Los Angeles, CA, USA

Abstract

Radiopharmaceutical analysis is limited by conventional methods. Radio-HPLC may be inaccurate for some compounds (e.g., ^{18}F-radiopharmaceuticals) due to radionuclide sequester. Radio-TLC is simpler, faster, and detects all species but has limited resolution. Imaging-based readout of TLC plates (e.g., using Cerenkov luminescence imaging) can improve readout resolution, but the underlying chromatographic separation efficiency may be insufficient to resolve chemically similar species such as product and precursor-derived impurities. This study applies a systematic mobile phase optimization method, PRISMA, to improve radio-TLC resolution. The PRISMA method optimizes the mobile phase by selecting the correct solvent, optimizing solvent polarity, and optimizing composition. Without prior knowledge of impurities and by simply observing the separation resolution between a radiopharmaceutical and its nearest radioactive or non-radioactive impurities (observed via UV imaging) for different mobile phases, the PRISMA method enabled the development of high-resolution separation conditions for a wide range of ^{18}F-radiopharmaceuticals ([^{18}F]PBR-06, [^{18}F]FEPPA, [^{18}F]Fallypride, [^{18}F]FPEB, and [^{18}F]FDOPA). Each optimization required a single batch of crude radiopharmaceutical and a few hours. Interestingly, the optimized TLC method provided greater accuracy (compared to other published TLC methods) in determining the product abundance of one radiopharmaceutical studied in more depth ([^{18}F]Fallypride) and was capable of resolving a comparable number of species as isocratic radio-HPLC. We used the PRISMA-optimized mobile phase for [^{18}F]FPEB in combination with multi-lane radio-TLC techniques to evaluate reaction performance during high-throughput synthesis optimization of [^{18}F]FPEB. The PRISMA methodology, in combination with high-resolution radio-TLC readout, enables a rapid and systematic approach to achieving high-resolution and accurate analysis of radiopharmaceuticals without the need for radio-HPLC.

mvandam@mednet.ucla.edu .

Keywords

Radiochemistry; radiopharmaceuticals; radio-TLC; high-resolution; PRISMA optimization

1. Introduction

The importance of radiopharmaceuticals in healthcare has boomed in recent years, especially with the development and regulatory approval of several novel positron-emission tomography (PET) tracers and targeted radiotherapeutics for neuroendocrine tumors and prostate cancer, illustrating the profound potential of theranostics and personalized medicine[1–6]. There have also been significant advances in new imaging agents to study, diagnose, and aid drug development for Alzheimer's disease[7–9], and discoveries of new oncologic targets that may lead to improved diagnostics and therapies for many types of cancer[10,11]. In support of these research and clinical uses, the analysis of radiolabelled species is vital in applications encompassing the development of novel radiopharmaceuticals (e.g., synthesis optimization)[12–16], quality control (QC) analysis of formulated radiopharmaceuticals[17,18], and the analysis of radiometabolites[19,20]. Separation can be challenging as impurities or metabolites may be numerous, and many may have structural similarities to the radiopharmaceutical.

Radiopharmaceutical analysis is traditionally performed using chromatographic methods such as radio high-performance liquid chromatography (radio-HPLC) and radio thin-layer chromatography (radio-TLC). Though it exhibits high resolution, radio-HPLC has been criticized because species such as [^{18}F]fluoride can be trapped in the column. Thus, based on detectors at the column output, the chromatogram may not accurately reflect the actual radiochemical composition[21]. Traditional radioactivity scanning readouts used in radio-TLC circumvent this issue by assessing the entire distribution of analytes along the whole plate. However, radio-TLC can suffer from lower resolution than radio-HLPC. Imaging-based TLC readout methods can improve readout resolution compared to scanning detectors[22,23]. Still, they may not offer improvement if the underlying chromatographic resolution of the separation process on the TLC plate is poor.

Though there is an optimum separation distance, with regards to separation efficiency and resolution, for each type of TLC plate[24], distances are often kept short in the radiochemistry field due to the strong dependence on of separation time on separation distance and the need for rapid separations when using short-lived radioisotopes. In principle, factors like stationary phase could be varied, but the radiochemistry field has predominantly used silica (normal-phase) plates[25–29] and, very occasionally, C18 (reverse-phase) plates[30]. This leaves mobile phase composition as the main adjustment to improve resolution.

Due to the limited knowledge of analytes (e.g., synthesis impurities or metabolites), it is often difficult to determine which mobile phases are most appropriate for crude radiopharmaceutical mixtures. Traditionally, mobile phases for radio-TLC are selected from the literature for a radiopharmaceutical structurally similar to the one of interest. Many reports use an organic solvent mixed with water (i.e., with the water added to increase

migration for highly polar species) [31–34]. However, we recently showed that water could lead to the complex behavior of species on the plate[35], including migration of multiple bands corresponding to [^{18}F]fluoride (normally sequestered at the origin), and purely organic mobile phases would be preferable.

A systematic approach called PRISMA was developed to facilitate optimal mobile phase selection without needing prior knowledge about the structures and properties of analytes[36]. Herein, we describe, for the first time in radiochemistry, the use of the PRISMA method for the rapid selection of mobile phase conditions to achieve baseline separation of the desired radiopharmaceutical from both radioactive impurities (e.g., free radionuclide and other radioactive species) and UV-active non-radioactive impurities (e.g., precursor or precursor-derived impurities). While the PRISMA method is widely used in analytical chemistry laboratories, it has never, to our knowledge, been used in the radiochemistry field. This may be due to the fact that available radio-TLC scanners only provide detection of radioactive species, which in general does not provide a sufficient number of visible high-abundance species to efficiently optimize the mobile phase. We overcome this limitation by integrating radiation detection and UV detection in a co-registered manner using multi-channel imaging-based readout of the developed TLC plates. Multiple radiopharmaceuticals with various chemical characteristics, prepared from crude radiosyntheses (which contain many impurities with high structural and chemical similarity to the desired product), are examined to illustrate the utility of the PRISMA approach.

2. Experimental

2.1 Materials

All reagents and solvents were obtained from commercial suppliers. 2,3-dimethyl-2-butanol (thexyl alcohol; anhydrous, 98%), 4,7,13,16,21,24-hexaoxa-1,10-diazabicyclo[8.8.8]hexacosane (Kryptofix 222, K222; 98%), acetic acid (AcOH; glacial, >99.9%), acetone (suitable for HPLC, >99.9%), acetonitrile (MeCN; anhydrous, 99.8%), ammonium molybdate (99.98% trace metal basis), cerium sulfate, cesium carbonate (Cs_2CO_3; 99.995%), chloroform (>99.5%, contains 100–200 ppm amylenes as stabilizer), dichloromethane (DCM; anhydrous, >99.8% contains 40–150 ppm amylene as stabilizer), diethyl ether (Et_2O; >99.9% inhibitor free), N,N-dimethylacetamide (DMA; extra dry, 99.8%), dimethylsulfoxide (DMSO; anhydrous, >99.9%), hydrochloric acid (HCl; 36.5–38%), methanol (MeOH; anhydrous, 99.8%), n-butanol (n-BuOH; anhydrous, 99.8%), n-hexane (98%), ninhydrin (used as a TLC stain), n-methyl-2-pyrrolidone (NMP; anhydrous, 99.5%), potassium carbonate (K_2CO_3; ACS grade, >99%), potassium bicarbonate ($KHCO_3$; >99.95%, trace metal basis), potassium oxalate monohydrate ($K_2C_2O_4$; ACS reagent, 99%), pyridine (anhydrous, 99.8%), sulfuric acid (99.9%), triethylamine (TEA; anhydrous, >99%), tetrahydrofuran (THF; anhydrous, >99.9% inhibitor free), tetrakispyridine copper(II) trifluoromethanesulfonate ($Cu(py)_4(OTf)_2$; 95%), toluene (anhydrous, 99.8%), and water (H_2O; suitable for ion chromatography) were purchased from Sigma-Aldrich (St. Louis, MO, USA). (S)-2,3-dimethoxy-5-[3-[[(4-methylphenyl)-sulfonyl]oxy]-propyl]-N-[[1-(2-propenyl)-2-pyrrolidinyl]methyl]-benzamide ([^{18}F]Fallypride precursor, >95%), 5-(3-fluoropropyl)-2,3-dimethoxy-N-(((2S)-1-(2-

propenyl)-2-pyrrolidinyl)methyl)benzamide (Fallypride reference standard, >95%), 2-((2,5-dimethoxybenzyl)(2-phenoxyphenyl)amino)-2-oxoethyl 4-methylbenzenesulfonate ([^{18}F]PBR-06 precursor, >95%), 2-fluoro-N-(2-methoxy-5-methoxybenzyl)-N-(2-phenoxyphenyl)acetamide (PBR-06 reference standard, >95%), acetamide, N-[2-[2-[[(4-methylphenyl)sylfonyl]oxy]ethoxy]phenyl]methyl]-N-(4-phenoxy-3-pyridinyl) ([^{18}F]FEPPA precursor, >90%), N-acetyl-N-(2-fluoroethoxybenzyl)-2-phenoxy-5-pyridinamine (FEPPA reference standard, >95%), 3-nitro-5-[2-(2-pyridinyl)ethynyl]benzonitrile ([^{18}F]FPEB precursor, >95%), 3-fluoro-5-[(pyridin-2-yl)ethynyl]benzonitrile (FPEB reference standard, >95%), ethyl-(2S)-3-[4,5-bis[(2-methylpropan-2-yl)oxycarbonyloxy]-2-trimethylstannylphenyl]-2-formamidopropanoate ([^{18}F]FDOPA precursor, >95%), (2S)-2-amino-3-(2-fluoro-4,5-dihydroxyphenyl)propanoic acid (FDOPA reference standard, >95%), and tetrabutylammonium bicarbonate (TBAHCO$_3$; 75 mM in ethanol), were purchased from ABX Advanced Biochemical Compounds (Radeberg, Germany). Silica gel 60 F_{254} sheets (aluminum backing, 5 cm × 20 cm) were purchased from Merck KGaA (Darmstadt, Germany). Silica with concentration zone (Silica 60 with diatomaceous earth zone), TLC plates, channeled F254, were purchased from Sorbtech (Norcross, GA, USA). Glass microscope slides (76.2 mm × 50.8 mm, 1 mm thick) were obtained from C&A Scientific (Manassas, VA, USA). UV-C lightbulbs (25W, 254 nm with socket) and pendant lamp sockets (light cord with on/off switch) were purchased from Amazon (Seattle, WA, USA).

No-carrier-added [^{18}F]fluoride was produced by the (p, n) reaction of [^{18}O]H_2O (98% isotopic purity, Huayi Isotopes Co., Changshu, Jiangsu, China) in an RDS-111 cyclotron (Siemens, Knoxville, TN, USA) at 11 MeV, using a 1.2-mL silver target with havar foil.

2.2 Preparation of radiopharmaceuticals and standard mixtures

A series of radiopharmaceuticals were prepared using droplet radiochemistry methods on Teflon-coated silicon surface tension trap chips[37–39] to illustrate PRISMA's ability to optimize mobile phases for radiopharmaceutical analysis. Detailed protocols for the preparation of [^{18}F]FEPPA, [^{18}F]PBR-06, [^{18}F]Fallypride, and [^{18}F]FDOPA have been previously reported[40,41].

Crude [^{18}F]FPEB was prepared by adding an 8 μL droplet of [^{18}F]fluoride/[^{18}O]H_2O (37–55 MBq [1–1.5 mCi]; mixed with 120 nmol of Cs_2CO_3 and 360 nmol of K222) and drying at 105 °C for 1 min. Then, the fluorination step was performed by adding a 10 μL droplet containing 200 nmol of FPEB precursor dissolved in DMSO to the dried [^{18}F]fluoride residue and reacting at 120 °C for 5 min. The crude product was collected by dispensing 10 μL of 9:1 (v/v) MeOH:H_2O to the reaction site and aspirating the volume. This process was repeated 6x for 60 μL of collected crude product.

Stock solutions of reference standards were prepared at 20 mM concentrations. 5 mg of Fallypride was added to 685 μL of MeOH. 5 mg of PBR-06 was added to 632 μL MeOH. 5 mg of FEPPA was added to 657 μL of MeOH. 5 mg of FPEB was added to 1130 μL of MeOH. 5 mg of FDOPA was added to 1167 μL of MeOH.

2.3 TLC spotting, developing, and readout

TLC plates were cut (L × W, 6 cm × 3 cm), then marked with a pencil at 1 cm (origin line) and 5 cm (development line) from the bottom edge. 1 μL of the relevant crude radiopharmaceutical sample was applied to the plate via a micro-pipette. Standard and precursor samples were spotted in adjacent individual lanes. The spots were then dried under a gentle stream of nitrogen for 1 min. After development using a PRISMA-determined mobile phase (see below), the plates were dried under a gentle stream of nitrogen for 3 min and then visualized via Cerenkov luminescence imaging (CLI)[22,42] with 1 min exposure and UV imaging for 7 ms exposure, as previously reported[35].

Following CLI and UV imaging, some cases used TLC stains by dipping the developed TLC plates in the stain of interest (Hanessian stain[43] or ninhydrin). Gentle heating of the TLC plate at 80 °C by a hot plate was used to stain the TLC plates. Hanessian stain was prepared according to the literature[44].

2.4 Radio-HPLC Analysis of [^{18}F]Fallypride

As a performance comparison, some crude [^{18}F]Fallypride microscale reactions were analyzed with radio-TLC and radio-HPLC. The radio-HPLC system setup comprised a Smartline HPLC system (Knauer, Berlin, Germany) equipped with a degasser (Model 5050), pump (Model 1000), UV detector (254 nm; Eckert & Ziegler, Berlin, Germany), gamma-radiation detector (BFC-4100, Bioscan, Inc., Poway, CA, USA), and counter (BFC-1000; Bioscan, Inc., Poway, CA, USA). A C18 Gemini column was used for separations (250 × 4.6 mm, 5 μm, Phenomenex, Torrance, CA, USA). Samples were separated with a mobile phase of 60% MeCN in 25 mM NH_4HCO_2 with 1% TEA (v/v) and a flow rate of 1.5 mL/min resulting in a retention time for [^{18}F]Fallypride of 5.8 min.

3. Methodology

3.1 Analysis of TLC plates

To determine the chromatographic resolution for the crude radiopharmaceutical lane on each plate, a MATLAB program with a graphical user interface (GUI) was developed (Supplementary Information Figure S1). Initially, the user is asked to select a CLI image file. The program performs background corrections as previously described[22,42], the user can scale the image by selecting an upper-intensity value. In the next step, the user selects the corresponding UV image file and is instructed to adjust the brightness and contrast through programmed slider controls. The adjusted CLI and UV images are combined into a composite black and white image (after inverting the pixel intensities of the UV image), which is used to define the lane for the automatic generation of CLI and UV line profiles (chromatograms). To select the lane's width, the user draws a line across the broadest chromatographic band in the composite image. Following this, the user is prompted to draw a line along the center of the lane.

To generate the CLI chromatogram, the program automatically creates a series of adjacent line profiles (image brightness versus distance along lane) at 1-pixel increments within the defined lane width and, from these, calculates an average line profile and then normalizes it

to the highest intensity analyte. This user-defined line profile is then displayed, enabling the user to set a threshold height for automated peak identification to ignore background noise. The MATLAB program performs automatic peak detection on the resultant chromatogram, then fits Gaussian curves to each peak and sums these to create a single multi-Gaussian fit.

A similar process is carried out to generate the UV chromatogram, except that an additional correction is made at the end to account for uneven UV illumination along the length of the lane. In the UV image, immediately adjacent to the user-selected lane, the program captures an additional 20 'background' line profiles just adjacent to each side of the selected lane and averages them together into a single 'background' line profile, which is subtracted from the initial UV chromatogram to give the final corrected UV chromatogram.

After fitting, the MATLAB program computes the centroid and full width half maximumfor each peak in the CLI and UV chromatograms, enabling the user to perform the standard calculation of chromatographic resolution between the radiopharmaceutical and the nearest impurity [45].

3.2 PRISMA optimization

The originally reported PRISMA method[36] was applied with minor modifications. The entire optimization process could be carried out with a single batch of crude radiopharmaceutical using twenty identically-prepared TLC plates in a few hours. Each plate was spotted with three lanes: the crude radiopharmaceutical, the precursor, and the reference standard.

Step 1: solvent selection—A total of eight plates were developed with pure solvents selected from Snyder selectivity groups[46] to compare separation resolution. The pure solvents selected were miscible with n-hexane (Supplemental Information Table S1). Based on a visual assessment of their ability to separate impurities (radioactive and non-radioactive) from the target radiopharmaceutical, three solvents (denoted for purposes of the following discussion as A, B, and C) exhibiting the highest degree of separation were chosen, where A, B, and C are listed in order of increasing solvent polarity. (It is expected that A, B, and C will be different for each different radiopharmaceutical studied.)

Step 2: solvent polarity optimization—To account for the intrinsic differences in solvent polarity, solvents are all 'normalized' to the same polarity before optimizing the solvent mixture. The polarity of a mixture (S_t) is simply the volumetric average of polarities of its constituents, i.e. $S_t = x*S_X + y*S_Y$, where × and y are the volume fraction of the two component solvents, and S_X and S_Y are the polarities of each of the two component solvents. N-hexane (solvent polarity = 0) was used as a dilutant to 'normalize' the solvent polarities to the same values. Recalling that the strength of the lowest polarity pure solvent (A) is S_A, diluted forms of the three solvents A, B, and C were prepared that all had strength S_A – 0.5. Similarly, another set of three diluted solvents A, B, C, all with strength S_A - 1.0, and a third set, all with strength S_A - 1.5, were prepared. For each of the three resulting strength values (S_A – 0.5, S_A - 1.0, and S_A - 1.5), the corresponding set of three diluted solvents were mixed in a 1:1:1 ratio, designated as 333 in selectivity point (P_s) notation, where the three digits represent the volume fraction of each of the diluted solvents (i.e., volume fraction ×

10 and then rounded to an integer value). 3 TLC plates were developed with these equal volume polarity-adjusted solvent mixtures. The optimal polarity was selected, so the desired radiopharmaceutical band was in the range $0.2 < R_f < 0.8$. If multiple solvent polarities mobilized the radiopharmaceutical into this range, the polarity with the greatest separation of the nearest impurity to the radiopharmaceutical was chosen for further optimization. Should none of the solvents mobilize the radiopharmaceutical to the desired range, the solvents that moved UV active impurities to the greatest degree were selected for further optimization.

Step 3: additive selection—Adding ionic pairing reagents (e.g., TEA and AcOH) can sometimes further improve separation resolution. This process was typically performed with only a few additional TLC plates. Due to the low concentration of these additives in the mobile phases, their polarities in PRISMA optimization are often treated as negligible (i.e., 0) and were included in the solvent mixture by simultaneously removing an equal volume of n-hexane from the mixture recipe[36]. Initially, the addition of each additive was tested at concentrations of 0.1%. Should the resolution or band shapes be improved (i.e., reduced tailing or fronting), proportions of 0.5% are additionally surveyed. Should additives in these low concentrations lead to no observable differences, additional concentrations at 5% are surveyed. Further optimization of the additive concentrations was dynamically determined if they led to heightened resolution of the radiopharmaceutical. (Though adding larger amounts of additives can have a non-negligible impact on the overall strength of the mixture, i.e. changing it slightly from the optimum determined in Step 2, the solvent mixture comparisons in Step 4 are all performed with the same proportion of additive and thus same overall mixture solvent strength, and useful interpolations can still be made.)

Step 4: composition optimization—Nine additional TLC plates were separated using different solvent compositions to optimize the mobile phase composition (P_s values of 100, 010, 001, 622, 262, 226, 406, 460, and 055, all at the previously selected optimal solvent strength and additive amount). The resolution was quantified for each lane. In addition to these selectivity points, we also included resolution data for the other selectivity points surveyed. We picked the mobile phase composition from this data set that gave the highest resolution, performing linear interpolation if needed (Supplementary Information Section S1.1).

3.3 Analysis of radiosynthesis performance

Analysis of reaction performance was performed as previously described[40]. Briefly, crude radiochemical yield (crude RCY) was calculated by multiplying the efficiency of collecting radioactivity from the chip, by the fluorination efficiency determined via TLC analysis.

4.0 Results and Discussion

The PRISMA method optimized radio-TLC mobile phases for several clinically-relevant radiopharmaceuticals with varying calculated properties (Table 1).

4.1 Optimization of separation of [^{18}F]Fallypride samples

Due to its moderate polarity and polar surface area, [^{18}F]Fallypride was selected as an initial model compound to undergo the PRISMA process (Figure 1A). The solvent-screening step revealed that n-BuOH (denoted as solvent A), THF (denoted as solvent B), and acetone (denoted as solvent C) provided the best separation of [^{18}F]Fallypride from impurities. Based on the minimum solvent strength of n-BuOH (3.9), the solvent polarities of 3.5, 3.0, and 2.5 were chosen for the survey at the equivolume mixture of strength-adjusted solvents (i.e., P_s = 333). While all the surveyed polarities led to the mobilization of [^{18}F]Fallypride in the R_f range of 0.2–0.8, S_t = 2.5 led to the greatest separation of [^{18}F]Fallypride from other analytes. Tailing of [^{18}F]Fallypride was observable with all mobile phases tested to this point. A possible explanation for this tailing could be ion pairing induced by interactions between the amide functional group of [^{18}F]Fallypride and surface silanol groups on the TLC plate. Different concentrations of TEA[47] were added in percentages of 0.1, 5, and 10% (v/v) to reduce ionic pairing across the plate during development. Using 10% (v/v) TEA led to well-defined bands and was used for further optimization. After surveying nine additional solvent mixtures (P_s), the optimal chromatographic resolution for [^{18}F]Fallypride from nearest impurity (R = 1.54) was found to be P_s = 055, S_t = 2.5 (Figure 1B). This selectivity point corresponds to a mobile phase composition of 31.3:24.5:34.3:10.0 (v/v) THF:acetone:n-hexane:TEA.

4.2 Comparison of optimized radio-TLC to radio-HPLC

We next compared the optimized TLC method with an isocratic HPLC method. While there are limitations of comparing a normal-phase TLC method with a reversed-phased HPLC method, which furthermore have very different migration lengths, we aimed only to compare the number of resolved species (which are likely in different orders), and the relative abundance of those species. This comparison is made because normal-phase TLC and reversed-phase HPLC (with similar migration lengths as used here) are by far the most predominantly used analytical methods in radiochemistry. A crude sample of [^{18}F]Fallypride was produced under droplet-radiochemistry conditions[40], modified to result in a low yield and high prevalence of side products. Briefly, increased $TBAHCO_3$ (300 vs. 240 nmol) was used in the [^{18}F]fluoride drying step, and the radiofluorination was performed with 100 nmol instead of 234 nmol of precursor and reacted at 140 °C for 10 min instead of 110 °C for 1 min. Interestingly, the optimized radio-TLC method separated the same number of radioactive analytes as radio-HPLC (Figure 2). We can see evidence, however, of the well-known underestimation of [^{18}F]fluoride in the radio-HPLC analysis[21]: the abundance of [^{18}F]fluoride computed from the radio-HPLC chromatogram is 71%, but, in comparison, was 95% when computed from the radio-TLC. Even more alarming, due to the underestimation of [^{18}F]fluoride, the apparent formation of [^{18}F]Fallypride calculated from the radio-HPLC chromatogram was nearly 7%, while it was <1% using radio-TLC (Table 2), suggesting more than a 7-fold error by radio-HPLC. However, if the discrepancy in the size of the [^{18}F]fluoride peaks is removed by ignoring this peak in both the radio-HPLC and radio-TLC chromatograms, the proportions of all other species are found to be similar, indicating excellent quantitative agreement between radio-HPLC and radio-TLC (with the PRISMA-optimized mobile phase).

Because of the excellent agreement, it is possible to consider using an imaging-based readout of TLC plates separated according to the PRISMA-optimized mobile phase as a simpler and more rapid alternative to radio-HPLC for radiopharmaceutical analysis. If multiple samples need to be analyzed, then the advantage of radio-TLC is further magnified as multiple samples can be spotted on the same plate and separated and read out in parallel[11]. In contrast, analyzing multiple samples via radio-HPLC requires ample time for cleaning and re-equilibration between samples.

4.3 Comparison of literature mobile phases to PRISMA-optimized mobile phase

The separation achieved with the PRISMA-optimized mobile phase was compared to mobile phases reported in the literature for the analysis of [^{18}F]Fallypride. We produced [^{18}F]Fallypride under previously-reported droplet radiochemistry conditions[40] modified to give a moderate yield and many side products. Specifically, the amount of $TBAHCO_3$ used in the [^{18}F]fluoride drying step was increased (from 240 to 800 nmol), and the fluorination was performed with 200 nmol instead of 234 nmol of precursor and reacted at 140 °C for 10 min instead of 110 °C for 1 min. Analysis was performed using TLC plates with pre-concentration zones, and the separation distance was extended from 4 to 5 cm to ensure the highest possible separation resolution in all cases. All lanes were spotted with 1 μL of the same crude reaction mixture. Figure 3 details the mobile phases surveyed, along with the obtained CLI images and generated chromatograms. For each mobile phase, we also performed separations using only [^{18}F]TBAF (Supplemental Information Figure S3) or [^{19}F]Fallypride (Supplemental Information Figure S4) to confirm the R_f values of these species. Abundances of species, computed from areas under peaks in the chromatograms, are summarized in Table 3. A significant disparity in the estimated abundance of [^{18}F]Fallypride and other species between different mobile phases is evident. Mobile phases with aqueous compositions (rows 3, 4, and 5) led to the greatest apparent abundance of [^{18}F]Fallypride (i.e., 66.1%, 82.7%, and 84.7%), while purely organic mobile phases (rows 1, 2) led to similar abundances of [^{18}F]Fallypride (i.e., 46.5%, 47.4%) compared to the PRISMA optimized mobile phase (row 6; [^{18}F]fallypride abundance 41.4%). The discrepancy in results obtained from the aqueous mobile phases is difficult to explain, but due to the high degree of band overlap (with a low number of resolved bands), there are likely species co-eluting with [^{18}F]Fallypride. The moderate discrepancy between the organic mobile phases suggests that the initial two literature mobile phases may result in incomplete separation of analytes, and an overlapping band may be counted with the [^{18}F]Fallypride band. Using the same crude [^{18}F]Fallypride sample, we performed a radio-HPLC separation, collected the [^{18}F]Fallypride fraction, and compared the activity to the injected activity. In addition to the high similarity between the radio-TLC and radio-HPLC chromatograms (Supplemental Information Figure S5), the abundance of collected [^{18}F]Fallypride was 40.2%, in excellent agreement with the abundance obtained from radio-TLC using the PRISMA-optimized mobile phase.

These results further underscore the problems of [^{18}F]fluoride retention on HPLC columns, which can lead to significant over-estimation errors of radiochemical species, especially low-abundance ones. Furthermore, the discrepancy when using different radio-TLC mobile phases, even for the identical sample, raises questions about the accuracy of reported

results using certain mobile phases and underscores the importance of ensuring high chromatographic resolution of the analysis method.

4.4 Optimization of separation of [^{18}F]PBR-06 samples

For crude samples of [^{18}F]PBR-06 (Supplemental Figure S6), the solvent screening step revealed that diethyl ether (denoted as solvent A), dichloromethane (denoted as solvent B), and chloroform (denoted as solvent C) exhibited the greatest separation of impurities from [^{18}F]PBR-06. Solvent polarities were normalized to 2.5, 2.0, and 1.5. With the solvents mixed in equal proportions (P_s = 333), the greatest separation of [^{18}F]PBR-06 from impurities was obtained with S_t = 2.5. Low amounts of AcOH and TEA (0.5%) were tested as chromatographic additives. The use of AcOH resulted in more observable UV-active impurities and a slightly higher chromatographic resolution for [^{18}F]PBR-06 than the use of TEA. After evaluating the impact of other mixtures of the solvents (tested at S_t = 2.5 using 0.5% AcOH (v/v)), the greatest resolution of [^{18}F]PBR-06 from nearest impurity (R = 1.84) was obtained at P_s = 333, S_t = 2.5 (Supplemental Figure S6). This selectivity point corresponds to a mobile phase composition of 29.8:26.9:20.4:22.85:0.05 (v/v) diethyl ether:dichloromethane:chloroform:n-hexane:AcOH.

4.5 Optimization of separation of [^{18}F]FEPPA samples

For samples of [^{18}F]FEPPA (Supplemental Figure S7), the solvent screening test revealed that n-BuOH (denoted as solvent A), THF (denoted as solvent B), and acetone (denoted as solvent C) provided the best separation of [^{18}F]FEPPA from impurities. These solvents were normalized to have polarities of 3.5, 3.0, and 2.5. In equivolume mixtures (P_s = 333), S_t = 2.5 showed the greatest separation of impurities from [^{18}F]FEPPA. A screening of additives revealed heightened resolution of [^{18}F]FEPPA from impurities using 1% TEA. Further solvent mixtures were tested (at S_t = 2.5 and with the addition of 1% TEA), and P_s = 262, S_t = 2.5 showed the greatest chromatographic resolution of [^{18}F]FEPPA from its nearest impurity (R = 2.07). This selectivity point corresponds to a mobile phase composition of 12.8:37.5:9.8:38.8:1 n-BuOH:THF:acetone:n-hexane:TEA (v/v).

4.6 Optimization of separation of [^{18}F]FDOPA samples

We next considered the two-step radiofluorination of [^{18}F]FDOPA (Supplemental Information Figure S8), in which the crude product contains a relatively nonpolar radioactive intermediate and the highly polar [^{18}F]FDOPA product. It is notoriously difficult to separate extremely polar compounds on normal phase silica TLC plates. For this reason, it is notable that the literature for [^{18}F]FDOPA analysis cites the use of reverse phase chromatography for radio-TLC analyses[48–50]. In the solvent-screening step, [^{18}F]FDOPA could not be mobilized, but using the criteria of the furthest migration of UV impurity bands from one another, we selected n-butanol (denoted as solvent A), THF (denoted as solvent B), and acetone (denoted as solvent C). The polarity of each pure solvent was normalized to 3.5, 3.0, and 2.5. When comparing solvent strengths (at P_s = 333), S_t = 3.5 led to the greatest degree of movement for UV impurities, but S_t = 3.0 led to more distinguishable peaks and was chosen for further optimization. High percentages of chromatographic additives were tested to address the tailing across the TLC plate. The best separation was found with AcOH in 30% abundance. After comparing different solvent mixtures, P_s = 333, (at

S_t = 3.0 at 30% AcOH) exhibited the greatest chromatographic resolution of [^{18}F]FDOPA from its nearest impurity (R = 1.18). This selectivity point corresponds to a mobile phase composition of 22.6:21.7:19.6:61:30 (v/v) n-butanol:THF:acetone:n-hexane:AcOH. While baseline resolution was not achieved, the resolution achieved may be sufficient for synthesis optimization or may be improved by adapting the PRISMA method to other types of TLC plates.

4.7 Optimization of separation of [^{18}F]FPEB samples

Simple leaving groups in aromatic substitutions, such as NO_2 groups, are commonly used to radiofluorinate radiopharmaceuticals. It is noteworthy that the separation of these radiopharmaceuticals and precursor structures is relatively difficult using HPLC. Thus the application of the PRISMA method to [^{18}F]FPEB (Supplemental Figure S9), which is produced via S_NAR of a NO_2 leaving group, serves as a good illustration of the high-resolution capabilities of PRISMA. The solvent screening step revealed that diethyl ether (denoted as solvent A), n-BuOH (denoted as solvent B), and acetone (denoted as solvent C) yielded the greatest separation of impurities from [^{18}F]FPEB. Normalizing the polarities of the solvents to 2.5, 2.0, and 1.5, a comparison of equivolume mixtures (P_s = 333) showed that the best separation could be achieved with S_t = 1.5. Evaluation of chromatographic additives showed a minor improvement when using 1% TEA. After comparing additional solvent mixtures, the P_s = 406 mixture (with S_t = 1.5, 1% TEA) exhibited the best resolution of [^{18}F]FPEB from the nearest impurity (R = 1.71). This selectivity point corresponds to a mobile phase composition of 21.4:17.6:60.0:1.0 diethyl ether:acetone:n-hexane:TEA (v/v).

4.8 Optimization of [^{18}F]FPEB radiosynthesis with high-resolution TLC analysis

As an example of how the PRISMA method can be used, we performed a high-throughput synthesis optimization of [^{18}F]FPEB using multi-reaction droplet-radiochemistry methods[40] and performed radio-TLC analysis of reactions in a multi-lane fashion[22] (8 samples per TLC plate) using the PRISMA-derived mobile phase. In the literature, harsh reaction conditions, like high temperature and base concentrations, lead to the formation of hydrolyzed impurities similar to the [^{18}F]FPEB[39,40], and HPLC analysis of crude microscale reactions (via flow-based reactor) of [^{18}F]FPEB shows closely eluting radioactive impurities[39], that may be difficult to resolve via TLC without careful optimization.

Initial microscale conditions were adapted by scaling down conditions reported in literature[51]. [^{18}F]fluoride (20–30 MBq) mixed with 500 nmol of the base was first dried at 105 °C for 1 min, and then a 10 μL droplet of precursor solution (containing 250 nmol) was added and reacted for 5 min at 140 °C. We first compared the use of different bases ($K_2C_2O_4$, K_2CO_3, $KHCO_3$, and Cs_2CO_3) and two different reaction solvents (DMSO and NMP), with n=2 replicates per condition (Figure 4A). Cs_2CO_3, in combination with DMSO, was selected for further optimization based on good crude RCY and low volatile loss (high collection efficiency). In optimization of the base amount (Figure 4B), 290 nmol was selected as the best compromise of good crude RCY and low volatile losses. From a comparison of the impact of precursor amount (Figure 4C), a high amount of precursor is needed to improve crude RCY. By replotting the results as a function of the base to

precursor ratio (Figure 4D), we noticed we achieved a similar yield with only 120 nmol of the precursor by lowering the amount of Cs_2CO_3 to 200 nmol. The reaction temperature was further optimized, revealing an optimal temperature of 140 °C (Figure 4E).

Under the optimized conditions, [^{18}F]FPEB could be produced in a crude RCY of ~16%, greater than other reported literature conditions (4–10%)[51–55]. Sixty-four reactions could be performed per day, and by employing multi-lane TLC using the optimized mobile phase, all samples each day could be analyzed within 60 min. In contrast, using radio-HPLC analysis would likely have significantly overestimated the product yield (due to loss of [^{18}F]fluoride in the column), and test reactions would have taken approximately 30–40 min each to analyze. Due to the limited half-life of F-18, only 12–16 samples could be practically analyzed each day if HPLC was used. Thus the study would have taken many more days, more batches of radioisotope (potentially adding other variables for which additional replicates are needed), and more labor hours.

4.9 Additional readout channels via staining

In addition to radiation readout (via Cerenkov imaging) and readout via UV imaging, additional chemical information can be gleaned from the TLC plate. Staining is a widely used method in TLC analysis that is inexpensive, can be used to detect low abundance analytes (via water-based stains like Hanessian), stain for specific functional groups (e.g., ninhydrin for the detection of amines), and detect analytes that are not UV-active. To demonstrate this principle, we employed TLC stains in the analysis of [^{18}F]PBR-06 and [^{18}F]Fallypride crude samples. In the samples of [^{18}F]PBR-06, few analytes can be visualized by UV analysis by TLC (Supplemental Figure S10). Hanessian staining reveals faint traces of additional impurities near the product band. Ninhydrin staining did not reveal additional bands (Supplemental Figure S10), but because it stains amine groups, this can help determine the potential identities of the bands. For [^{18}F]Fallypride, Hanessian staining revealed no additional impurities (Supplementary Figure S11). Ninhydrin staining revealed a previously unseen impurity (Supplementary Figure S11).

Staining methods pose an interesting method to visualize low-abundance species and to glean additional chemical information about specific bands that could help to identify bands and improve understanding of competing reaction pathways. It is striking that the additional impurities detected via staining were well separated from the radiopharmaceutical, even though they were not visible during the PRISMA procedure to optimize the mobile phase.

5. Conclusions

In this study, a systematic mobile phase selection process, PRISMA, was applied to optimize TLC mobile phases to separate crude samples of radiopharmaceuticals. The PRISMA method provided a systematic framework to rapidly (<4 h) and efficiently (with only 1 batch of the crude radiopharmaceutical) reach a set of development conditions resulting in high-resolution separation without prior knowledge of impurity identities or properties. The method was successfully applied to multiple examples of diverse radiopharmaceuticals, achieving baseline separation of the radiopharmaceutical from radioactive and non-radioactive impurities. In the case of [^{18}F]Fallypride, the optimized

radio-TLC method rivaled the resolution of isocratic radio-HPLC while resulting in a more accurate analysis as the method does not suffer from the issue of loss of [^{18}F]fluoride to the column of radio-HPLC. Notably, the optimized TLC conditions can be applied for synthesis optimization and potentially to portions of QC testing (e.g., radiochemical purity) or radio-metabolite studies. [56–64] UV imaging and TLC staining can reveal additional species that are not visible with the traditional use of radio-TLC. This streamlined methodology can be easily employed by radiochemistry labs, using ubiquitous materials, and enabling anyone to develop high-resolution TLC separation methods for accurate radiopharmaceutical analysis.

Supplementary Material

Refer to Web version on PubMed Central for supplementary material.

Acknowledgments

The authors thank Jeffrey Collins for providing [^{18}F]fluoride for these studies. The authors also thank Judah Farahi for the precursor and standard material for synthesizing [^{18}F]FPEB. This work was supported in part by the National Cancer Institute (R21 CA212718), the National Institute of Biomedical Imaging and Bioengineering (R21 EB024243, R01 EB032264, and T32 EB002101), and the National Institutes of Health (S10 OD026942).

REFERENCES

[1]. Hofman MS, Kong G, Neels OC, Eu P, Hong E, Hicks RJ, High management impact of Ga-68 DOTATATE (GaTate) PET/CT for imaging neuroendocrine and other somatostatin expressing tumours, Journal of Medical Imaging and Radiation Oncology. 56 (2012) 40–47. 10.1111/j.1754-9485.2011.02327.x. [PubMed: 22339744]

[2]. Baum RP, Kulkarni HR, THERANOSTICS: From Molecular Imaging Using Ga-68 Labeled Tracers and PET/CT to Personalized Radionuclide Therapy - The Bad Berka Experience, Theranostics. 2 (2012) 437–447. 10.7150/thno.3645. [PubMed: 22768024]

[3]. Graf J, Pape U-F, Jann H, Denecke T, Arsenic R, Brenner W, Pavel M, Prasad V, Prognostic Significance of Somatostatin Receptor Heterogeneity in Progressive Neuroendocrine Tumor Treated with Lu-177 DOTATOC or Lu-177 DOTATATE, Eur J Nucl Med Mol Imaging. 47 (2020) 881–894. 10.1007/s00259-019-04439-9. [PubMed: 31414209]

[4]. Bräuer A, Grubert LS, Roll W, Schrader AJ, Schäfers M, Bögemann M, Rahbar K, 177Lu-PSMA-617 radioligand therapy and outcome in patients with metastasized castration-resistant prostate cancer, Eur J Nucl Med Mol Imaging. 44 (2017) 1663–1670. 10.1007/s00259-017-3751-z. [PubMed: 28624848]

[5]. Carlucci G, Ippisch R, Slavik R, Mishoe A, Blecha J, Zhu S, 68Ga-PSMA-11 NDA Approval: A Novel and Successful Academic Partnership, Journal of Nuclear Medicine. 62 (2021) 149–155. 10.2967/jnumed.120.260455. [PubMed: 33443068]

[6]. Keam SJ, Piflufolastat F 18: Diagnostic First Approval, Mol Diagn Ther. 25 (2021) 647–656. 10.1007/s40291-021-00548-0. [PubMed: 34292532]

[7]. Chiaravalloti A, Danieli R, Lacanfora A, Palumbo B, Caltagirone C, Schillaci O, Usefulness of 18F Florbetaben in Diagnosis of Alzheimer's Disease and Other Types of Dementia, Curr Alzheimer Res. 14 (2017) 154–160. 10.2174/1567205013666160620114309. [PubMed: 27334940]

[8]. Filippi L, Chiaravalloti A, Bagni O, Schillaci O, 18F-labeled radiopharmaceuticals for the molecular neuroimaging of amyloid plaques in Alzheimer's disease, Am J Nucl Med Mol Imaging. 8 (2018) 268–281. [PubMed: 30245918]

[9]. Lohith TG, Bennacef I, Vandenberghe R, Vandenbulcke M, Salinas CA, Declercq R, Reynders T, Telan-Choing NF, Riffel K, Celen S, Serdons K, Bormans G, Tsai K, Walji A, Hostetler ED, Evelhoch JL, Laere KV, Forman M, Stoch A, Sur C, Struyk A, Brain Imaging of Alzheimer Dementia Patients and Elderly Controls with 18F-MK-6240, a PET Tracer

Targeting Neurofibrillary Tangles, J Nucl Med. 60 (2019) 107–114. 10.2967/jnumed.118.208215. [PubMed: 29880509]

[10]. Treglia G, Muoio B, Roustaei H, Kiamanesh Z, Aryana K, Sadeghi R, Head-to-Head Comparison of Fibroblast Activation Protein Inhibitors (FAPI) Radiotracers versus [18F]F-FDG in Oncology: A Systematic Review, International Journal of Molecular Sciences. 22 (2021) 11192. 10.3390/ijms222011192. [PubMed: 34681850]

[11]. Dendl K, Koerber SA, Kratochwil C, Cardinale J, Finck R, Dabir M, Novruzov E, Watabe T, Kramer V, Choyke PL, Haberkorn U, Giesel FL, FAP and FAPI-PET/CT in Malignant and Non-Malignant Diseases: A Perfect Symbiosis?, Cancers. 13 (2021) 4946. 10.3390/cancers13194946. [PubMed: 34638433]

[12]. Rios A, Wang J, Chao PH, van Dam RM, A novel multi-reaction microdroplet platform for rapid radiochemistry optimization, RSC Adv. 9 (2019) 20370–20374. 10.1039/C9RA03639C. [PubMed: 35514735]

[13]. Wang M, Gao M, Miller KD, Zheng Q-H, Synthesis of [11C]PBR06 and [18F]PBR06 as agents for positron emission tomographic (PET) imaging of the translocator protein (TSPO), Steroids. 76 (2011) 1331–1340. 10.1016/j.steroids.2011.06.012. [PubMed: 21756927]

[14]. Chang C-W, Chiu C-H, Lin M-H, Wu H-M, Yu T-H, Wang P-Y, Kuo Y-Y, Huang Y-Y, Shiue C-Y, Huang W-S, Yeh SH-H, GMP-compliant fully automated radiosynthesis of [18F]FEPPA for PET/MRI imaging of regional brain TSPO expression, EJNMMI Res. 11 (2021) 26. 10.1186/s13550-021-00768-9. [PubMed: 33725191]

[15]. de Laat B, Leurquin-Sterk G, Celen S, Bormans G, Koole M, Laere KV, Casteels C, Preclinical evaluation and quantification of 18F-FPEB as a radioligand for PET imaging of the metabotropic glutamate receptor 5, J Nucl Med. (2015) jnumed.115.162636. 10.2967/jnumed.115.162636.

[16]. Shen B, Ehrlichmann W, Uebele M, Machulla H-J, Reischl G, Automated synthesis of n.c.a. [18F]FDOPA via nucleophilic aromatic substitution with [18F]fluoride, Applied Radiation and Isotopes. 67 (2009) 1650–1653. 10.1016/j.apradiso.2009.03.003. [PubMed: 19433364]

[17]. Dahlbom M, PET Calibration, Acceptance Testing, and Quality Control, in: Basic Science of PET Imaging, Springer, Cham, 2017: pp. 229–255. 10.1007/978-3-319-40070-9_10.

[18]. Fermi E, Quality Control of PET Radiopharmaceuticals, in: Molecular Imaging: Radiopharmaceuticals for PET and SPECT, Springer Berlin Heidelberg, 2009: pp. 197–204. 10.1007/978-3-540-76735-0_13 (accessed June 21, 2013).

[19]. Peyronneau M-A, Saba W, Goutal S, Kuhnast B, Dollé F, Bottlaender M, Valette H, [18F]Fallypride: Metabolism studies and quantification of the radiotracer and its radiometabolites in plasma using a simple and rapid solid-phase extraction method, Nuclear Medicine and Biology. 40 (2013) 887–895. 10.1016/j.nucmedbio.2013.06.003. [PubMed: 23891202]

[20]. Patt M, Schildan A, Barthel H, Becker G, Schultze-Mosgau MH, Rohde B, Reininger C, Sabri O, Metabolite analysis of [18F]Florbetaben (BAY 94–9172) in human subjects: a substudy within a proof of mechanism clinical trial, J Radioanal Nucl Chem. 284 (2010) 557–562. 10.1007/s10967-010-0514-8.

[21]. Ory D, Van den Brande J, de Groot T, Serdons K, Bex M, Declercq L, Cleeren F, Ooms M, Van Laere K, Verbruggen A, Bormans G, Retention of [18F]fluoride on reversed phase HPLC columns, Journal of Pharmaceutical and Biomedical Analysis. 111 (2015) 209–214. 10.1016/j.jpba.2015.04.009. [PubMed: 25898315]

[22]. Wang J, Rios A, Lisova K, Slavik R, Chatziioannou AF, van Dam RM, High-throughput radio-TLC analysis, Nuclear Medicine and Biology. 82–83 (2020) 41–48. 10.1016/j.nucmedbio.2019.12.003.

[23]. Ha YS, Lee W, Jung J-M, Soni N, Pandya DN, An GI, Sarkar S, Lee WK, Yoo J, Visualization and quantification of radiochemical purity by Cerenkov luminescence imaging, Anal. Chem. 90 (2018) 8927–8935. 10.1021/acs.analchem.8b01098. [PubMed: 29991252]

[24]. Spangenberg B, Poole CF, Weins C, Theoretical Basis of Thin Layer Chromatography (TLC), in: Spangenberg B, Poole CF, Weins C (Eds.), Quantitative Thin-Layer Chromatography: A Practical Survey, Springer, Berlin, Heidelberg, 2011: pp. 13–52. 10.1007/978-3-642-10729-0_2.

[25]. Ryzhikov NN, Seneca N, Krasikova RN, Gomzina NA, Shchukin E, Fedorova OS, Vassiliev DA, Gulyás B, Hall H, Savic I, Halldin C, Preparation of highly specific radioactivity [18F]flumazenil

and its evaluation in cynomolgus monkey by positron emission tomography, Nuclear Medicine and Biology. 32 (2005) 109–116. 10.1016/j.nucmedbio.2004.11.001. [PubMed: 15721755]

[26]. Vaulina D, Nasirzadeh M, Gomzina N, Automated radiosynthesis and purification of [18F]flumazenil with solid phase extraction, Applied Radiation and Isotopes. 135 (2018) 110–114. 10.1016/j.apradiso.2018.01.008. [PubMed: 29413823]

[27]. Nasirzadeh M, Vaulina DD, Kuznetsova OF, Gomzina NA, A novel approach to the synthesis of [18F]flumazenil, a radioligand for PET imaging of central benzodiazepine receptors, Russ Chem Bull. 65 (2016) 794–800. 10.1007/s11172-016-1376-1.

[28]. Inkster J. a. H., Akurathi V, Sromek AW, Chen Y, Neumeyer JL, Packard AB, A non-anhydrous, minimally basic protocol for the simplification of nucleophilic 18 F-fluorination chemistry, Scientific Reports. 10 (2020) 6818 (9 pages). 10.1038/s41598-020-61845-y. [PubMed: 32321927]

[29]. Ismail R, Irribarren J, Javed MR, Machness A, van Dam M, Keng PY, Cationic imidazolium polymer monoliths for efficient solvent exchange, activation and fluorination on a continuous flow system, RSC Advances. 4 (2014) 25348–25356. 10.1039/c4ra04064c.

[30]. Mandap KS, Ido T, Kiyono Y, Kobayashi M, Lohith TG, Mori T, Kasamatsu S, Kudo T, Okazawa H, Fujibayashi Y, Development of microwave-based automated nucleophilic [18F]fluorination system and its application to the production of [18F]flumazenil, Nuclear Medicine and Biology. 36 (2009) 403–409. 10.1016/j.nucmedbio.2009.01.011. [PubMed: 19423008]

[31]. Lazari M, Collins J, Shen B, Farhoud M, Yeh D, Maraglia B, Chin FT, Nathanson DA, Moore M, van Dam RM, Fully Automated Production of Diverse 18F-Labeled PET Tracers on the ELIXYS Multireactor Radiosynthesizer Without Hardware Modification, J. Nucl. Med. Technol. 42 (2014) 203–210. 10.2967/jnmt.114.140392. [PubMed: 25033883]

[32]. Ungersboeck J, Philippe C, Haeusler D, Mitterhauser M, Lanzenberger R, Dudczak R, Wadsak W, Optimization of [11C]DASB-synthesis: Vessel-based and flow-through microreactor methods, Applied Radiation and Isotopes. 70 (2012) 2615–2620. 10.1016/j.apradiso.2012.08.001. [PubMed: 22940416]

[33]. Koivula T, Laine J, Lipponen T, Perhola O, Kämäräinen E-L, Bergström K, Solin O, Assessment of labelled products with different radioanalytical methods: study on 18F-fluorination reaction of 4-[18F]fluoro-N-[2-[1-(2-methoxyphenyl)-1-piperazinyl]ethyl-N-2-pyridinyl-benzamide (p-[18F]MPPF), J Radioanal Nucl Chem. 286 (2010) 841–846. 10.1007/s10967-010-0802-3.

[34]. Yu H-M, Chan C-H, Yang C-H, Hsia H-T, Wang M-H, Hexavalent lactoside labeled with [18F]AlF for PET imaging of asialoglycoprotein receptor, Applied Radiation and Isotopes. 162 (2020) 109199. 10.1016/j.apradiso.2020.109199. [PubMed: 32501233]

[35]. Laferriere-Holloway TS, Rios A, Van Dam RM, Detrimental impact of aqueous mobile phases in 18F-labelled radiopharmaceutical analysis via radio-TLC, RSC Analytical Methods. (Submitted).

[36]. Nyiredy S, Planar Chromatographic Method Development Using the PRISMA Optimization System and Flow Charts, Journal of Chromatographic Science. 40 (2002) 553–563. 10.1093/chromsci/40.10.553. [PubMed: 12515358]

[37]. Wang J, Chao PH, van Dam RM, Ultra-compact, automated microdroplet radiosynthesizer, Lab Chip. (2019) 2415–2424. 10.1039/C9LC00438F. [PubMed: 31187109]

[38]. Wang J, Holloway T, Lisova K, van Dam RM, Green and efficient synthesis of the radiopharmaceutical [18F]FDOPA using a microdroplet reactor, React. Chem. Eng. (2019). 10.1039/C9RE00354A.

[39]. Wang J, Chao PH, Slavik R, van Dam RM, Multi-GBq production of the radiotracer [18F]fallypride in a droplet microreactor, RSC Adv. 10 (2020) 7828–7838. 10.1039/D0RA01212B. [PubMed: 35492189]

[40]. Rios A, Holloway TS, Chao PH, De Caro C, Okoro CC, van Dam RM, Microliter-scale reaction arrays for economical high-throughput experimentation in radiochemistry, Sci Rep. 12 (2022) 10263. 10.1038/s41598-022-14022-2. [PubMed: 35715457]

[41]. Lu Y, van Dam RM, First microvolume metal-mediated synthesis of [18F]FDOPA in a microreactor [ABSTRACT], Nuclear Medicine and Biology. 96–97 (2021) S15–S16. 10.1016/S0969-8051(21)00291-2.

[42]. Dooraghi AA, Keng PY, Chen S, Javed MR, Kim C-J"CJ", Chatziioannou AF, van Dam RM, Optimization of microfluidic PET tracer synthesis with Cerenkov imaging, Analyst. 138 (2013) 5654–5664. 10.1039/C3AN01113E. [PubMed: 23928799]

[43]. Appendix 3: Recipes For TLC Stains, in: The Synthetic Organic Chemist's Companion, John Wiley & Sons, Ltd, 2007: pp. 171–172. 10.1002/9780470141045.app3.

[44]. Cai L, Thin Layer Chromatography, Current Protocols Essential Laboratory Techniques. 8 (2014) 6.3.1–6.3.18. 10.1002/9780470089941.et0603s08.

[45]. U.S. Pharmacopeia (USP), Chapter 621: Chromatography, (2021). https://www.usp.org/sites/default/files/usp/document/harmonization/gen-chapter/harmonization-november-2021-m99380.pdf (accessed November 14, 2022).

[46]. Snyder L, Solvent selectivity in normal-phase TLC, Journal of Planar Chromatography – Modern TLC. 21 (2008) 315–323. 10.1556/JPC.21.2008.5.1.

[47]. Fried B, Sherma B, Thin-Layer Chromatography, Revised And Expanded, CRC Press, Boca Raton, 1999. 10.1201/9780203910214.

[48]. Huang Y-Y, Tzen K-Y, Liu Y-L, Chiu C-H, Tsai C-L, Wen H-P, Tang K-H, Liu C-C, Shiue C-Y, Impact of residual 18F-fluoride in 18F-FDOPA for the diagnosis of neuroblastoma, Ann Nucl Med. 29 (2015) 489–498. 10.1007/s12149-015-0970-x. [PubMed: 25851249]

[49]. Huang Y-Y, Poniger S, Tsai C-L, Tochon-Danguy HJ, Ackermann U, Yen R-F, Three-step two-pot automated production of NCA [18F]FDOPA with FlexLab module, Applied Radiation and Isotopes. 158 (2020) 108871. 10.1016/j.apradiso.2019.108871. [PubMed: 32113705]

[50]. Nanabala R, Pillai MRA, Gopal B, Experience of 6-l-[18F]FDOPA Production Using Commercial Disposable Cassettes and an Automated Module, Nucl Med Mol Imaging. 56 (2022) 127–136. 10.1007/s13139-022-00742-w. [PubMed: 35607634]

[51]. Wang J-Q, Tueckmantel W, Zhu A, Pellegrino D, Brownell A-L, Synthesis and preliminary biological evaluation of 3-[18F]fluoro-5-(2-pyridinylethynyl)benzonitrile as a PET radiotracer for imaging metabotropic glutamate receptor subtype 5, Synapse. 61 (2007) 951–961. 10.1002/syn.20445. [PubMed: 17787003]

[52]. Varlow C, Murrell E, Holland JP, Kassenbrock A, Shannon W, Liang SH, Vasdev N, Stephenson NA, Revisiting the Radiosynthesis of [18F]FPEB and Preliminary PET Imaging in a Mouse Model of Alzheimer's Disease, Molecules. 25 (2020) 982. 10.3390/molecules25040982. [PubMed: 32098347]

[53]. Sullivan JM, Lim K, Labaree D, Lin S, McCarthy TJ, Seibyl JP, Tamagnan G, Huang Y, Carson RE, Ding Y-S, Morris ED, Kinetic Analysis of the Metabotropic Glutamate Subtype 5 Tracer [18F]FPEB in Bolus and Bolus-Plus-Constant-Infusion Studies in Humans, J Cereb Blood Flow Metab. 33 (2013) 532–541. 10.1038/jcbfm.2012.195. [PubMed: 23250105]

[54]. Liang SH, Yokell DL, Jackson RN, Rice PA, Callahan R, Johnson KA, Alagille D, Tamagnan G, Collier TL, Vasdev N, Microfluidic continuous-flow radiosynthesis of [18F]FPEB suitable for human PET imaging, Med. Chem. Commun. 5 (2014) 432–435. 10.1039/C3MD00335C.

[55]. Lim K, Labaree D, Li S, Huang Y, Preparation of the metabotropic glutamate receptor 5 (mGluR5) PET tracer [18F]FPEB for human use: An automated radiosynthesis and a novel one-pot synthesis of its radiolabeling precursor, Applied Radiation and Isotopes. 94 (2014) 349–354. 10.1016/j.apradiso.2014.09.006. [PubMed: 25305528]

[56]. Li F, Hicks JW, Yu L, Desjardin L, Morrison L, Hadway J, Lee T-Y, Plasma radio-metabolite analysis of PET tracers for dynamic PET imaging: TLC and autoradiography, EJNMMI Research. 10 (2020) 141 (12 pages). 10.1186/s13550-020-00705-2. [PubMed: 33226509]

[57]. Jin Z-H, Furukawa T, Sogawa C, Claron M, Aung W, Tsuji AB, Wakizaka H, Zhang M-R, Boturyn D, Dumy P, Fujibayashi Y, Saga T, PET imaging and biodistribution analysis of the effects of succinylated gelatin combined with l-lysine on renal uptake and retention of 64Cu-cyclam-RAFT-c(-RGDfK-)4 in vivo, European Journal of Pharmaceutics and Biopharmaceutics. 86 (2014) 478–486. 10.1016/j.ejpb.2013.11.006. [PubMed: 24316338]

[58]. Kokic M, Honer M, Kessler LJ, Grauert M, Schubiger PA, Ametamey SM, Synthesis and in Vitro and in Vivo Evaluation of [11c]methyl-Biii277cl for Imaging the Pcp-Binding Site of the Nmda Receptor by Pet, Journal of Receptors and Signal Transduction. 22 (2002) 123–139. 10.1081/RRS-120014591. [PubMed: 12503611]

[59]. Kuang Y, Salem N, Corn DJ, Erokwu B, Tian H, Wang F, Lee Z, Transport and Metabolism of Radiolabeled Choline in Hepatocellular Carcinoma, Mol. Pharmaceutics. 7 (2010) 2077–2092. 10.1021/mp1001922.

[60]. Kuang Y, Wang F, Corn DJ, Tian H, Lee Z, Metabolism of Radiolabeled Methionine in Hepatocellular Carcinoma, Mol Imaging Biol. 16 (2014) 44–52. 10.1007/s11307-013-0678-z. [PubMed: 23921714]

[61]. Matusch A, Meyer PT, Bier D, Holschbach MH, Woitalla D, Elmenhorst D, Winz OH, Zilles K, Bauer A, Metabolism of the A1 adenosine receptor PET ligand [18F]CPFPX by CYP1A2: implications for bolus/infusion PET studies, Nuclear Medicine and Biology. 33 (2006) 891–898. 10.1016/j.nucmedbio.2006.07.006. [PubMed: 17045169]

[62]. Roivainen A, Någren K, Hirvonen J, Oikonen V, Virsu P, Tolvanen T, Rinne JO, Whole-body distribution and metabolism of [N-methyl-11C](R)-1-(2-chlorophenyl)-N-(1-methylpropyl)-3-isoquinolinecarboxamide in humans; an imaging agent for in vivo assessment of peripheral benzodiazepine receptor activity with positron emission tomography, Eur J Nucl Med Mol Imaging. 36 (2009) 671–682. 10.1007/s00259-008-1000-1. [PubMed: 19050880]

[63]. Tang D, Li J, Buck JR, Tantawy MN, Xia Y, Harp JM, Nickels ML, Meiler J, Manning HC, Evaluation of TSPO PET Ligands [18F]VUIIS1009A and [18F]VUIIS1009B: Tracers for Cancer Imaging, Mol Imaging Biol. 19 (2017) 578–588. 10.1007/s11307-016-1027-9. [PubMed: 27853987]

[64]. Steinmetz A, The Broad Scope of Cesium Salts in Organic Chemistry, Catalysts Cesium from Acros Organics. (2011) 3–11.

[65]. López-López E, Naveja JJ, Medina-Franco JL, DataWarrior: an evaluation of the open-source drug discovery tool, Expert Opinion on Drug Discovery. 14 (2019) 335–341. 10.1080/17460441.2019.1581170. [PubMed: 30806519]

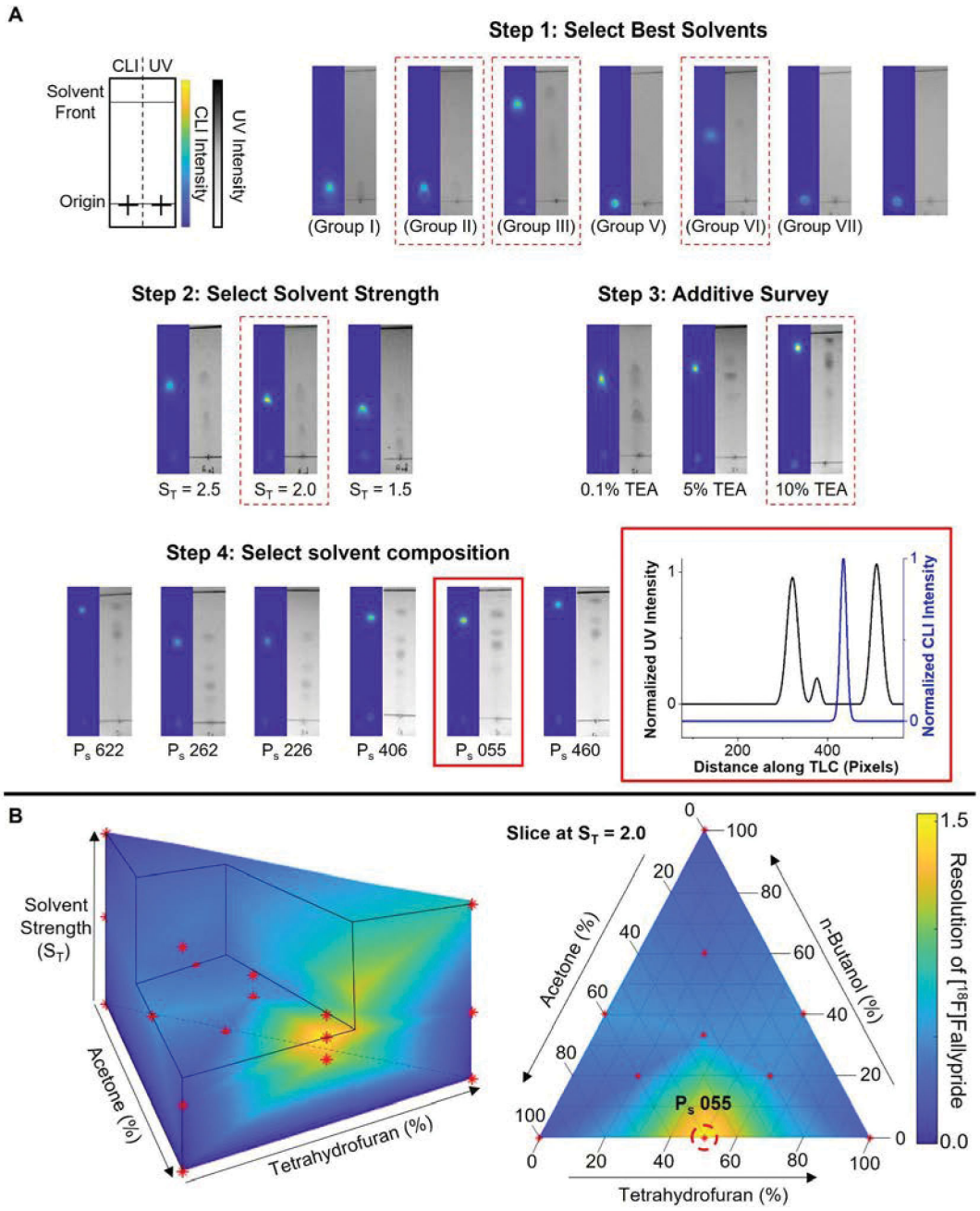

Figure 1.

(A) The PRISMA method comprises several stages of mobile phase optimization to determine conditions that provide the best resolution. TLC plates prepared with mixtures of [^{18}F]Fallypride and impurities are separated under different conditions and visualized via CLI and UV imaging. A custom software program computes the resolution between the radiopharmaceutical and the nearest impurity (radioactive or non-radioactive). Dashed red lines denote the optimal selection from each stage of the process, and the inset shows a chromatogram from the final optimized conditions. (B) The resolution is mapped as a function of mobile phase composition and solvent strength (left), and a slice of this prism

taken at the optimal solvent strength (2.0) shows how resolution varies as a function of composition (right).

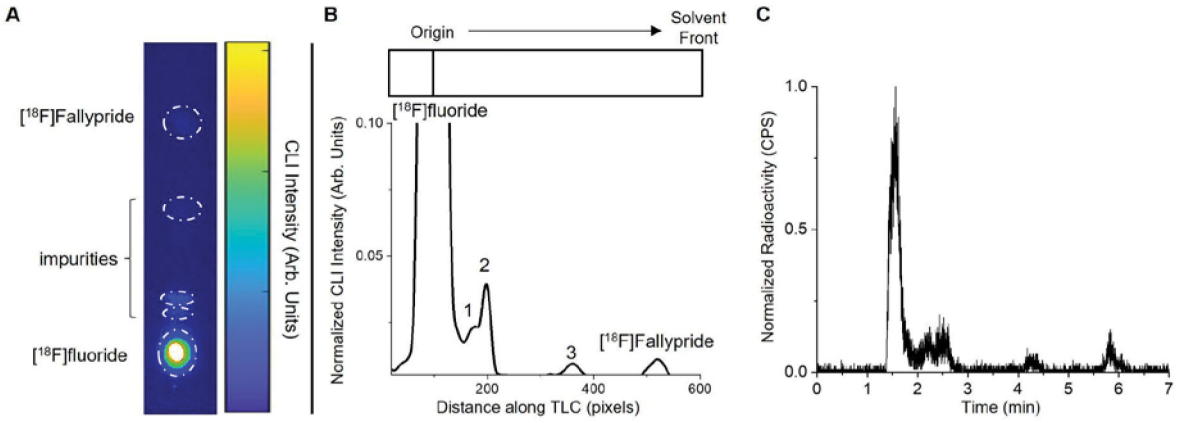

Figure 2.

(A) Cerenkov luminescence image of a TLC plate after spotting with a crude [^{18}F]Fallypride sample and separation via the PRISMA-optimized mobile phase. (B) TLC chromatogram was generated by taking a line profile of the Cerenkov luminescence image along the lane. The chromatogram is truncated to better show the smaller peaks. (C) Isocratic radio-HPLC chromatogram of the same sample.

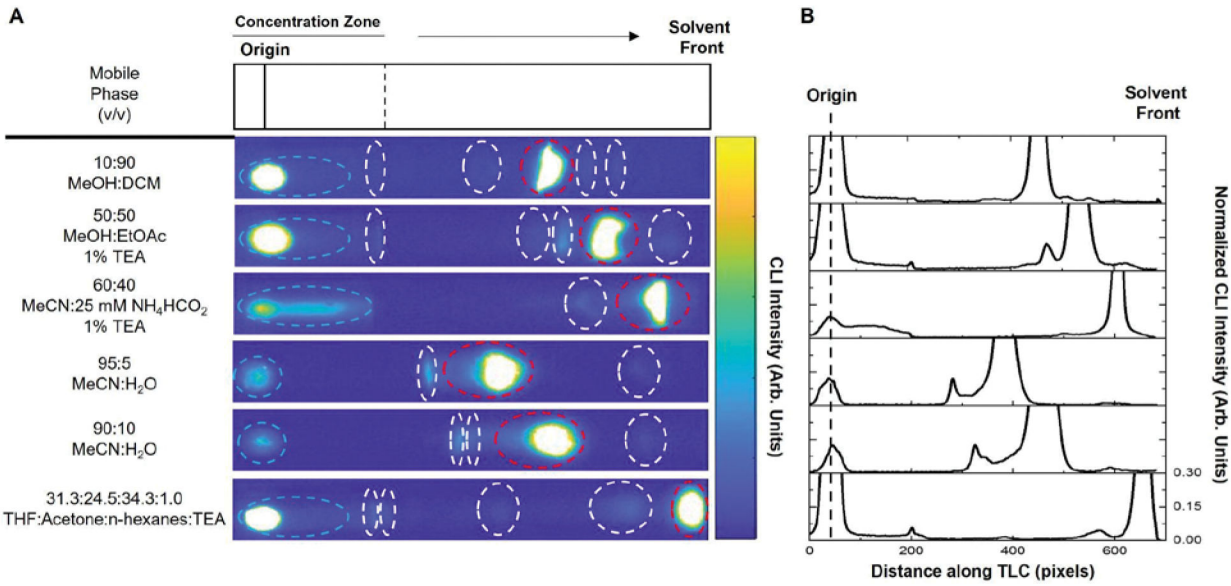

Figure 3.

(A) CLI images of TLC plates spotted with crude [^{18}F]Fallypride and developed with different mobile phases from literature (first five entries) and the PRISMA-derived mobile phase (last entry). [^{18}F]fluoride is denoted with dashed blue ellipses, side-products denoted with dashed white ellipses, and [^{18}F]Fallypride denoted with dashed red ellipses. (B) TLC chromatograms were generated by taking a line profile of the Cerenkov luminescence images. Chromatograms are truncated to better show the smaller peaks.

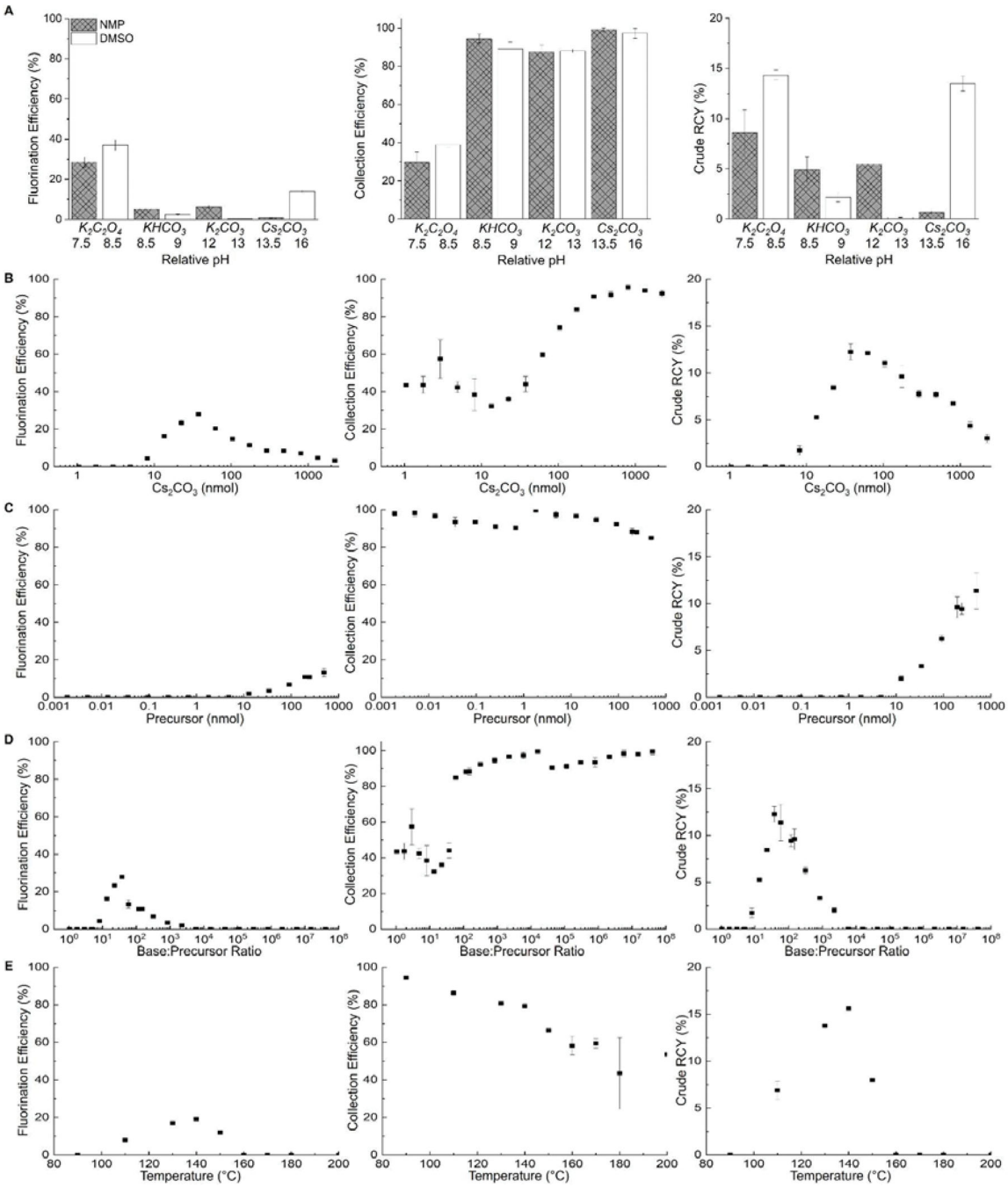

Figure 4.

Optimization of the synthesis of [^{18}F]FPEB (n = 2), leveraging high-throughput analyses enabled by multi-lane radio-TLC using the PRISMA-optimized mobile phase. Reaction volume is 10 μL and reaction time is 5 min in all cases. (A) Impact of different bases and two different reaction solvents. Relative pH is shown below each data point.[53] Precursor amount: 250 nmol, base amount: 500 nmol, reaction temperature: 140 °C. (B) Effect of the amount of Cs_2CO_3. Precursor amount: 250 nmol, reaction temperature: 140 °C. (C) Effect of precursor amount. Cs_2CO_3 amount: 290 nmol, reaction temperature: 140 °C. (D) Data from

B and C were replotted to show the effect of the base:precursor ratio. (E) Effect of reaction temperature. Precursor amount: 200 nmol, Cs_2CO_3 amount: 120 nmol.

Table 1.

Selected radiopharmaceuticals and their calculated properties. cLogP denotes the calculated partition coefficient (a measure of the lipophilicity) of the radiopharmaceutical, and TPSA denotes the total polar surface area of the radiopharmaceutical. Properties were calculated using the open-source software DataWarrior[65].

Radiopharmaceutical	cLogP	TPSA	H-Bond Donor Count	H-Bond Acceptor Count
[^{18}F]PBR-06	4.6	48.0	0	5
[^{18}F]FEPPA	3.6	51.7	0	5
[^{18}F]Fallypride	3.3	50.8	1	5
[^{18}F]FPEB	2.7	36.7	0	3
[^{18}F]FDOPA	−2.0	104.0	4	6

Table 2.

Comparison of the radiochemical composition of a crude [^{18}F]Fallypride sample as determined by radio-TLC and radio-HPLC.

	Integration (%)			
Peak	**HPLC^{A}**	**HPLC^{B}**	**TLC^{A}**	**TLC^{B}**
[^{18}F]fluoride	70.5	-	94.7	-
1	8.7	29.9	1.6	30.7
2	11.0	37.2	2.4	36.3
3	3.3	11.0	0.6	11.6
[^{18}F]Fallypride	6.5	22.0	0.8	21.3

^{A}Estimation accounts for all peaks, including [^{18}F]fluoride

^{B}Estimation ignores [^{18}F]fluoride and is calculated solely based on other peaks

Table 3.

Integration of analytes detected by radio-TLC in the analysis of [^{18}F]Fallypride.

Mobile Phase (v/v)	Number of Observable Peaks	Abundance (%)						Fallypride R_f
				Impurities				
		[^{18}F]fluoride	[^{18}F]Fallypride	1	2	3	4	
10:90 MeOH:DCM[16]	6	46.7	46.5	1.7	2.0	1.3	1.8	0.65
50:50 MeOH:EtOAc 1% TEA[17]	6	43.9	47.4	0.7	1.7	4.7	1.7	0.76
60:40 MeCN:25 mM NH_4HCO_2 1% TEA[11,34]	3	30.4	66.1	3.6	-	-	-	0.87
95:5 MeCN:H_2O[19]	4	9.6	82.7	6.6	1.1	-	-	0.55
90:10 MeCN:H_2O[35]	4	6.9	84.7	4.3	2.3	-	-	0.66
31.3:24.5:34.3:1.0 THF:acetone:n-hexane:TEA	6	49.8	41.4	2.3	1.0	1.5	4.0	0.91